Indoor mm-Wave Channel Measurements: Comparative Study of 2.9 GHz and 29 GHz

Ozge Hizir Koymen, Andrzej Partyka, Sundar Subramanian, Junyi Li
Qualcomm R&D, Bridgewater, New Jersey

***Abstract*—The millimeter-wave (mm-Wave) frequency band (~30-300 GHz) has received significant attention lately as a prospective band for 5G systems. Millimeter-wave frequencies have traditionally been used for backhaul, satellite and other fixed services. While these bands offer substantial amount of bandwidth and opportunity for spatial multiplexing, the propagation characteristics for terrestrial mobile usage need to be fully understood prior to system design. Towards this end, this paper presents preliminary indoor measurement results obtained using a channel sounder equipped with omni- and directional antennas at 2.9 GHz and 29 GHz as a comparative study of the two bands. The measurements are made within a Qualcomm building in Bridgewater, NJ, USA, for two separate floors, each representing a different yet representative type of office plan. We present measurements and estimated parameters for path loss, excess delay, RMS delay and analyze the power profile of received paths. In addition, we present several spherical scans of particular links to illustrate the 3-D angular spread of the received paths. This work represents initial results of an ongoing effort for comprehensive indoor and outdoor channel measurements. The measurements presented here, along with cited references, offer interesting insights into propagation conditions (e.g. loss, delay/angular spread etc.), coverage and robustness for mobile use of millimeter-wave bands. We believe additional extensive measurement campaigns in diverse settings by academia and industry would help facilitate the generation of usable channel models.**

I. Introduction

There is a growing demand for high data rates spurred by a variety of mobile applications ranging from always-on data for cloud services, high quality video conferencing to on-demand movies for mobile consumption. To satisfy the ever-increasing data demand, the next generation technology (5G) may support radically different techniques than current generations. Recent trends in RF technology have enabled the production of cost-effective radios capable of operating in carrier frequencies well above the traditional sub-6 GHz bands[1]. For example, the WiGiG/802.11ad standard has been defined and products based on this standard are currently available, though mainly geared towards very short range applications (e.g. cable replacement, wireless docking, etc.)[2]. The use of higher frequencies (>10 GHz), approaching millimeter-wave (mm-Wave), to enable cellular data access is gaining support and is widely considered to play an important part of next generation wireless technologies [3], [4].

The millimeter-wave bands benefit from the availability of large amounts of underutilized spectrum [5] (over 1.3 GHz available in the 28 GHz band, 1.4 GHz in the 39 GHz band, and almost 7 GHz of spectrum in the 60 GHz band). The advantages of operating at a higher frequency are not just the increased bandwidth but also the following: (i) the capability of antennas to attain higher directivity at higher frequencies (for the same aperture size) enables the inherent beamforming to improve the signal strength and spectral efficiency, (ii) the narrower beams also provide an opportunity for denser spatial reuse. While these advantages exist, the characterization of the basic propagation behavior of wireless signals is essential in determining the usefulness of these bands. Electromagnetic propagation in mm-Wave bands is different from the sub-6 GHz bands; the size of typical objects in the environment are much larger compared to the wavelength at these higher frequencies. The reflection and diffraction properties of everyday objects are different and absorption losses are also higher [6], [3]. Outdoor-to-Indoor signal penetration is also expected to be weaker at mm-Wave bands. Thus, it remains to be seen through careful measurements whether these bands can be of practical value for cellular access. A particular mm-Wave frequency of interest is the 28 GHz band. The band was originally allocated for Local Multipoint Distribution Systems (LMDS), but a large number of licenses have been returned due to insufficient use [7].

Conducting well-planned and detailed measurement campaigns is an extremely valuable method to understanding the mm-Wave channel. Many research teams and universities have performed channel sounding and channel characterization for the 28 GHz band. Details of an outdoor measurement campaign at 28GHz along with results obtained are presented in [8]. The derived channel parameters were described in [9]. A summary of these measurements can be found in [3]. A few other research teams in Samsung [10] and Ericsson [11] have also reported some preliminary measurement results. While outdoor propagation characterization is valuable, the use of millimeter wave base-stations for indoor small cells is also an appealing use-case. There has been some prior work on indoor propagation measurements of mm-Wave frequencies (a few in 28 GHz [10], and in 60 GHz [12], [13]).

In our paper, we report our results from an indoor measurement campaign at 29 GHz band using a channel sounder outfitted with omni- and directional antennas. We measure channel characteristics such as pathloss, delay spread, distribution of power over received paths among other quantities. We also measure these properties at 2.9 GHz (at the same locations) to provide a side-by-side contrast of propagation at those frequencies.

978-1-4799-5952-5/15/$31.00 ©2015 IEEE

II. Measurement Setup and Methodology

A. Channel Sounder

We developed a custom mobile test system which includes a channel sounder with automatic elevation and azimuth scan capability. The transmitter and receiver are battery equipped and can be moved about freely. The channel sounder operates at 2.9GHz and 29GHz; switching between the frequencies does not require reconnecting of cables or antennas. The resolution of the channel sounder is approximately 5ns; additional improvement is possible through post-processing of raw data. We collect parallel data sets for 2.9GHz and 29GHz at identical locations with omni-directional antennas. In addition, we collect data using directional horn antennas with 10dB and 20dB gain at 29GHz. For the spherical scans, we scan in both azimuth 360° and in elevation from -30° to +90°. The resultant scans includes 39 slices with a 10dB gain antenna and 331 slices with a 20dB gain antenna.

B. Measurement Methodology and Scenarios

The indoor measurements were made on two floors of the Qualcomm building in Bridgewater, NJ, USA, with dimensions of 75m (W) x 40m (L). The two floors, whose floorplans are exhibited in Figures 1 and 2, represent two types of typical office environments. The third floor is mostly comprised of cubicles (Figure 3) along the edge of the floorplan with walled offices and conference rooms towards the center. The fourth floor, shown in Figure 4, is comprised of walled offices (larger than the third floor), conference rooms and laboratories.

The building construction is representative of a modern office building in the United States. The partition walls are constructed with steel beams spaced at 1.5ft (.46m) intervals. The ceiling is a dropped ceiling ~9ft (2.7m) above the floor with an additional ~3ft (.91m) cavity below the concrete ceiling. While the cavity is not a visible aspect of the office, it does play an important role in the propagation measurements as presented later. A visual inspection of the cavity verifies the abundance of metal objects in a fairly open space with minimal correspondence to the office partition below. Of particular importance is the concrete ceiling with a corrugated metal substrate (Figure 5) and the numerous metal ductwork pipes (Figure 6).

On the third floor, the measurements were made between two transmitter locations (red stars) and the same 37 receiver locations. The first transmit location is centrally located while the second one is positioned at the lefthand edge of the floor plan (see Figure 1). On the fourth floor, the measurements were made between a single transmitter location and 44 receiver locations. Given the high density of partition walls in the office building, a large majority of the measurements were non-line-of-sight (NLOS) in nature.

To facilitate unimpeded measurements of path loss without shadowing induced by humans, most measurements were made during non-office hours. Measurements were repeated several times at the same location to average over dynamic influences. Each receiver location was also measured at five

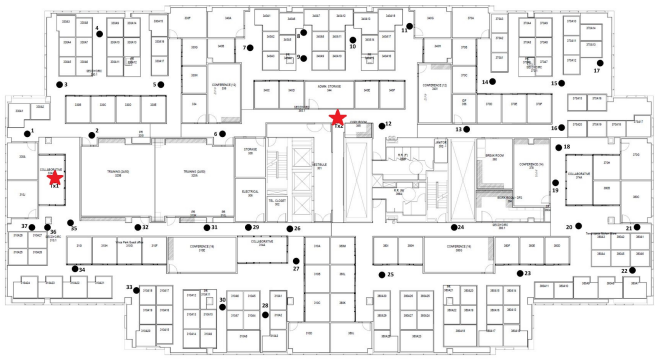

Fig. 1. Third Floor Measurement Locations

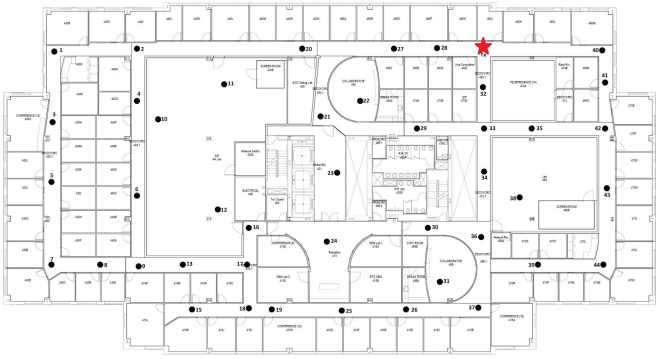

Fig. 2. Fourth Floor Measurement Locations

separate locations offset from each other (center of a circle with a radius of 18 cm along with 4 points on the circumference) to get diversity in measurement and avoid possible nulls in the channel response. Both 2.9 GHz and 29 GHz measurements were made at the same locations to get an exact correspondence.

The transmit and receive antennas were placed 10 inches (24.4 cm) and 29 inches (73.4 cm) below the dropped ceiling, respectively, to avoid any interaction with measurement equipment. For each captured channel response, a maximum of 15 samples were classified as legitimate paths. The minimum power requirement for such classification was set to be min(12 dB SNR, 20 dB below the largest path) where the SNR is referenced post processing gain.

III. Results

The following subsections present analysis for path loss, delay, received path power profile and spherical scans. While relevant metrics differ slightly between the two measurement floors, it was concluded that a combined analysis would be representative of an indoor office scenario. Particular differences between the floors and their effect on metrics is discussed in the subsections when relevant. Furthermore, the measurements do not represent a sufficient number of line-of-sight (LOS) links to make a full generalization but do look representative and are presented to add value to the discussion.

Fig. 3. Third Floor Cubicle

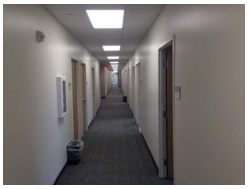

Fig. 4. Fourth Floor Hallway

Fig. 5. Dropped Ceiling Cavity

Fig. 6. Dropped Ceiling Ductwork

A. Path Loss Analysis

We collected total received power from omni-directional antenna measurements to estimate the path loss model for both 2.9 GHz and 29 GHz. For LOS links, the path loss is fit to the following log-linear model

$$PL(d)_{[dB]} = PL(d_0)_{[dB]} + \beta \log_{10}(d/d_0) + X, \quad X \sim \mathcal{N}(0, \sigma^2) \quad (1)$$

where $PL(d_0)_{[dB]}$ is the reference path loss at the reference distance of d_0, β is the path loss exponent (PLE), X is a random variable with a Normal distribution that models the lognormal shadowing. For the subsequent models, we took the reference distance d_0 as 1m. Furthermore, we removed the reference path loss $PL(d_0)_{[dB]}$ from the measurement data to normalize the path loss to $0dB$ at d_0 for both 2.9 GHz and 29 GHz to allow for direct comparison. An estimate of the PLE and lognormal shadowing are obtained through a least square fit of the parameters to the measurement data.

For NLOS links, the path loss empirical data indicates a distinctive dual slope path loss model. While this dual slope behavior was initially thought to be an artifact at 29 GHz, measurements at 2.9 GHz were verified to exhibit the same behavior. The dual slope model therefore looks to be a characteristic of the measurement environment and link distance and not mm-Wave specific. A close inspection of the floor plans reveals that all but one of the links below $10m$ is associated with Tx1 on the third floor. The shorter distance links around this transmitter appear to be neither strictly LOS or NLOS with some of the receiver locations obstructed by a single blocking material (i.e., pane of glass, partition wall,etc.).

For the dual slope path loss model, Equation 1 represents the path loss in the region $(d_0 \leq d \leq d_t)$. The second slope, valid in the region $d > d_t$, is represented by

$$PL_1(d)_{[dB]} = PL(d_t)_{[dB]} + \beta_1 \log_{10}(d/d_t) + X_1, \quad X_1 \sim \mathcal{N}(0, \sigma_1^2), \quad (2)$$

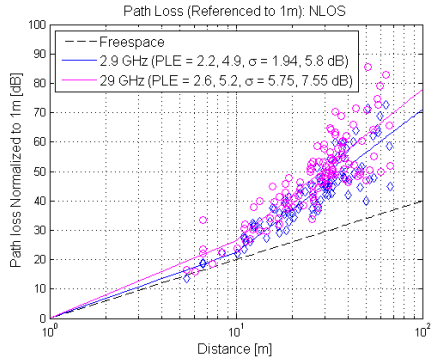

(a) NLOS

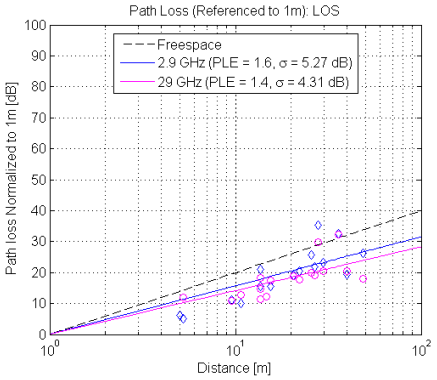

(b) LOS

Fig. 7. Estimated Path Loss Model along with Measurement Data (Actual PL = [reference loss at 1m for a given frequency] + [normalized PL as presented])

where d_t is the threshold distance at which the the two models intercept. Note that $PL_1(d_t)_{[dB]} = PL(d_t)_{[dB]}$ to avoid a discontinuity in the dual slope model. The threshold distance d_t was found to be $10m$ through minimization of the mean square error of the estimated path loss model and the empirical data.

An alternate approach to modeling the indoor path loss is of the form represented by the Motley-Keenan [14] or COST 231 multi-wall [15] models. Fitting to this type of model however requires significant additional work to model the environment (enumeration of partition types, assignment of loss factors, etc...) and added complexity in applying the model.

The dual slope NLOS and the single slope LOS path loss models can be seen in Figure 7. We note that the path loss exponent for the NLOS model does not vary greatly between 2.9 GHz and 29 GHz although the lognormal shadowing standard deviation is considerably larger for 29 GHz. A larger path loss exponent is expected due to the number of partition walls in between the links and the material properties at 29 GHz; the path loss at 2.9 GHz however is not substantially lower. We attribute this observation to the type of construction and the cavity above the dropped ceiling. While there are numerous partitions with highly absorbent and reflective materials, the cavity above represents an open space, likely allowing for a significant mode of propagation at 29 GHz.

The LOS behavior points to a waveguide-like affect of

transmitting down long hallways; this is particularly applicable for the 4th floor given the long continuous hallways (Figure 4). The path loss exponents are seen to be much better than free space for both 2.9 GHz and 29 GHz. Both the PLE and the lognormal shadowing standard deviation appears to be smaller for 29 GHz suggesting a better waveguiding effect at mmWave bands.

We next studied the validity of a distance independent log-normal shadowing model. We calculated the standard deviation of the lognormal shadowing using a sliding window of length 10. The resultant data points along with a linear fit are shown in 8 for both NLOS and LOS. The standard deviation for both types of links exhibit a clear distance dependency. The shadowing standard deviation for NLOS was fit to a dual slope model to minimize the mean square error of the fit. The threshold distance was found to be $d = 30m$ for both frequency bands and likely related to the physical structure of the environment. The standard deviation appears to be fairly flat before the threshold distance and then increases by ~8 dB over the remaining 40m. For LOS links, the change across the measurement distances is about ~4 dB. There appears to be a clear justification for a distant dependent lognormal shadowing model. It should be noted that the behavior is exhibited both at 2.9 GHz and 29 GHz. However, unlike a 2.9 GHz system, the measurement range for 29 GHz defines the limit of a typical mm-Wave link budget. We believe, therefore, that it is important to get the path loss model accurate in this limited range for mm-Wave to evaluate system capacity and performance accurately.

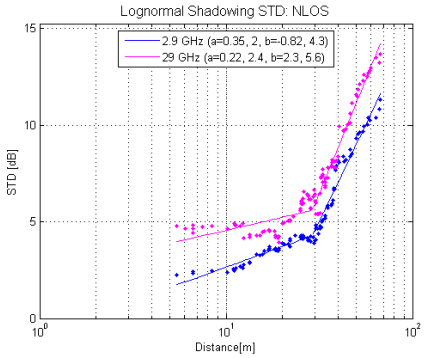

(a) NLOS

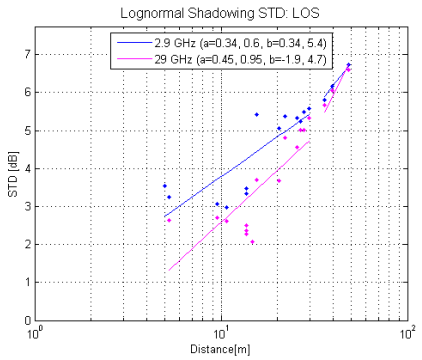

(b) LOS

Fig. 8. Standard Deviation of the Lognormal Shadow Fading

B. Delay Analysis

In this subsection we analyze the excess delay and RMS delay spread of the omni-directional antenna measurement data with some comparison to directional measurements. For reference, given the dimensions of the building, the longest end-to-end delay is $250ns$; any delay beyond this value is a result of reflections. For excess delay, we fit an exponential distribution to the data for each link type and frequency band. The distributions for the combined third and fourth floors measurements can be seen in Figure 9 for 29 GHz. Results for 2.9 GHz are not shown in the figures but also follow an exponential distribution with $\lambda^{-1} = 114ns$ and $\lambda^{-1} = 67.9ns$ for NLOS and LOS, respectively. The cumulative density functions of the RMS delay spread for the combined third and fourth floor measurements are shown in Figure 10(a).

For NLOS, the mean of the excess delay and RMS delay spread is less at 29 GHz as expected given the difference in propagation characteristics. For LOS, the mean of the excess delay is actually higher at 29 GHz. The RMS delay spread for LOS illustrates this difference through a heavier tail with larger delay. This behavior is due to a better wave-guide effect resulting in more reflective paths propagating across the link distance with significant power.

We also compared the RMS delay spread for omni-directional and directional (20 bBi) receive antennas at 29 GHz for 34 NLOS Rx locations. The results in Figure 10(b), illustrate that for indoor office NLOS measurements, directional receive antennas do not reduce the RMS delay spread as might be expected. This result validates the applicability of our omni-directional delay analysis even for systems utilizing beamforming at the receiver.

C. Path Power Analysis

We diverge from the comparative study of the previous sections and only consider 29 GHz for the received path power analysis. The longer wavelength at 2.9 GHz makes it unfeasible to resolve individual paths through narrow beams with a reasonable antenna aperture. There are corner cases (i.e., angles of arrival separated by 120°) that would allow for separation but not in the general case. On the contrary, it is quite feasible to beamform to an individual path at 29 GHz.

We do not have full spherical scans for each of the receive locations which would ideally be needed for a proper power analysis through the use of a clustering algorithm; this task is planned for completion in the near future. Our limited analysis has shown however that looking at the top two strongest taps of an omni-directional antenna response is generally associated with two separate paths (angles of arrivals). We generalize this observation by assuming the first and second path always represents different angles of arrival with the caveat that they may not actually be resolvable in reality.

We present two statistics, the power of the strongest path and the ratio of the second and first strongest paths. The power

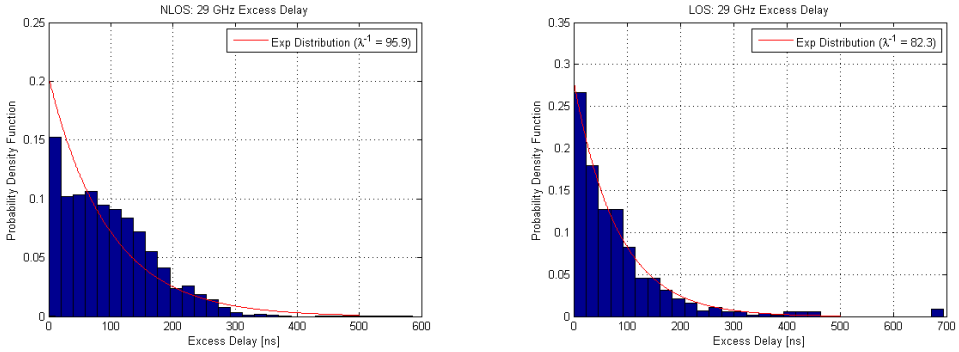

(a) NLOS

(b) LOS

Fig. 9. Excess Delay Distribution along with Empirical Data (29 GHz)

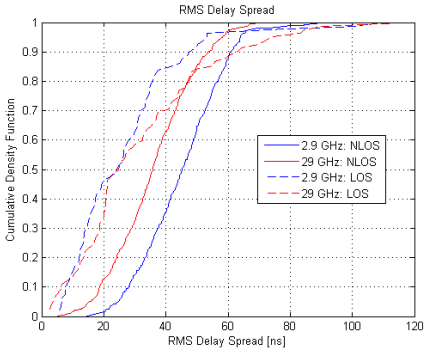

(a) Omni-directional Distributions

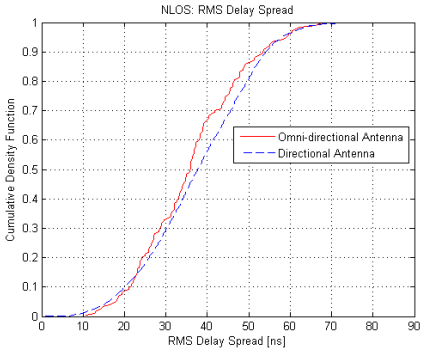

(b) Omni-directional and Directional Comparison at 29 GHz

Fig. 10. RMS Delay Distribution

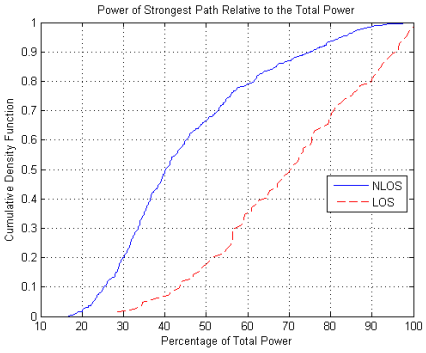

Fig. 11. Power of Strongest Path at 29 GHz

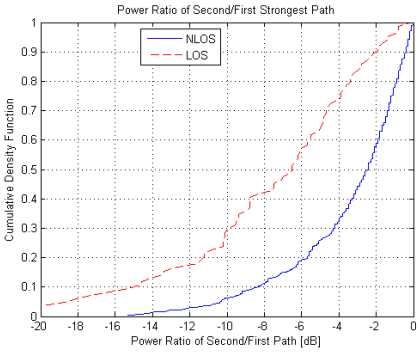

Fig. 12. Power of Ratio of Second/First Strongest Paths at 29 GHz

of the strongest path gives an idea of the potential diversity in the environment or the availability of alternate paths with significant power. The ratio of the two paths gives an idea of how viable a single alternative path is to sustain a link or alternately how concentrated the remaining power is on the secondary path. Figures 11 and 12 shows the CDF plots for combined third and fourth floor measurements.

D. Spherical Scans

In addition to the omni-directional antenna measurements presented, we performed a set of spherical scans with both 20 dBi and 10 dBi directional horn antennas at a subset of the receiver locations. The objective of these scans is twofold, to collect statistics for angular information and to investigate the appropriateness of a 2-D or 3-D channel model.

We present two representative spherical scans with a 20 dBi horn antenna from the fourth floor in Figure 13. The scans are displayed as actual measured power without any normalization to a reference distance. Each scan represents a different link and only shows a single directional view. The chosen view represents the more interesting aspect of the scan but does not imply the absence of energy on the reverse side. A large

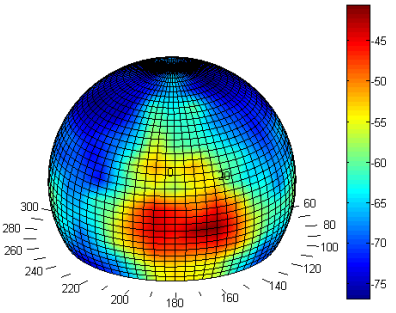

(a) Scan 1

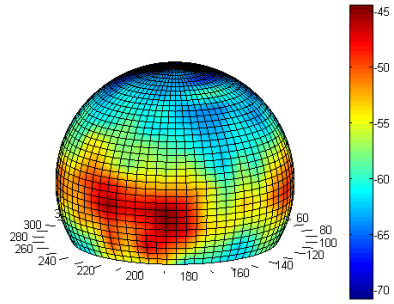

(b) Scan 2

Fig. 13. Spherical Scans from the Fourth Floor

majority of the spherical scans display significant energy over a full 360° of the azimuth angle.

The presented scans illustrate the diversity in receive angle for both azimuth and elevation. Figure 13(a) represents a scan with significant elevation energy with the main path close to 0° above the horizon and two separate paths at about 45° above the horizon. We attribute at least some these higher elevation paths to propagation through the dropped ceiling cavity. Figure 13(b) illustrates a scenario of significant energy spread around a wide azimuth angle spread.

The scans suggest rays arrive at receiver location over a large spread in azimuth and elevation angles. There are certainly scans that do not exhibit much variance in elevation but a significant number of scans do. This may not be representative of other measurement environments but certainly holds true of our chosen office environment for both floorplans. The scans suggest a 3D channel model is the appropriate choice for modeling indoor mm-Wave propagation.

IV. Conclusion

The work presented in this paper is intended to offer some insight into millimeter-wave propagation within a typical indoor office building environment. The comparative study of 2.9 GHz and 29 GHz provides a convenient way to contrast 29GHz propagation to the community already familiar with sub-6GHz bands. The work highlighted the differences in propagation characteristics at 29 GHz. Certain metrics such as path loss behavior were found to vary less than expected between the two bands. On the other hand, particular differences in delay metrics between NLOS and LOS links emphasized some basic differences between the bands.

The results in this paper represent an initial result of an ongoing indoor and outdoor campaign. For the indoor campaign, analysis of the spherical scans will lead to a continued refinement of the metrics along with an improved understanding of indoor millimeter-wave propagation. We emphasize that a complete understanding of indoor and outdoor propagation on the way to a full channel model is beyond the scope of just a single measurement campaign. Results from the cited measurement campaigns highlight differences as strongly as consensus, illustrating the need for further extensive measurements in diverse settings.

Acknowledgment

The authors would like to acknowledge the contribution of Ashwin Sampath, Juergen Cezanne, John Sanelli and Nilay Shahof (all members of Qualcomm R&D group in Bridgewater, NJ, USA).

References

[1] Ali M Niknejad and Hossein Hashemi. *mm-Wave Silicon Technology*. Springer, 2008.

[2] Wilocity. `http://wilocity.com/products/chipsets`.

[3] Theodore S Rappaport, Shu Sun, Rimma Mayzus, Hang Zhao, Yaniv Azar, Kevin Wang, George N Wong, Jocelyn K Schulz, Mathew Samimi, and Felix Gutierrez. Millimeter wave mobile communications for 5G cellular: It will work! *Access, IEEE*, 1:335–349, 2013.

[4] Zhouyue Pi and Farooq Khan. An introduction to millimeter-wave mobile broadband systems. *Communications Magazine, IEEE*, 49(6):101–107, 2011.

[5] FCC. http://transition.fcc.gov/bureaus/oet/tac/--tacdocs/meeting61313/TACPresentations6-13-13.pdf.

[6] Zhao Qingling and Jin Li. Rain attenuation in millimeter wave ranges. In *Antennas, Propagation EM Theory, 2006. ISAPE '06. 7th International Symposium on*, pages 1–4, Oct 2006.

[7] FCC. Memorandum opinion and order: Da 14-782. 2014.

[8] Yaniv Azar, George N Wong, Kevin Wang, Rimma Mayzus, Jocelyn K Schulz, Hang Zhao, Felix Gutierrez, DuckDong Hwang, and Theodore S Rappaport. 28 ghz propagation measurements for outdoor cellular communications using steerable beam antennas in new york city. In *Communications (ICC), 2013 IEEE International Conference on*, pages 5143–5147. IEEE, 2013.

[9] Mustafa Riza Akdeniz, Yuanpeng Liu, Shu Sun, Sundeep Rangan, Theodore S Rappaport, and Elza Erkip. Millimeter wave channel modeling and cellular capacity evaluation. *arXiv preprint arXiv:1312.4921*, 2013.

[10] Kyoungtae Lee Jung-Hoon Ko Sooyoung Hur, Yeon-Jea Cho and Jeongho Park. Millimeter-wave channel modeling based on measurements in in-building and campus environments at 28 ghz. 2014. http://www.ic1004.org/uploads/Abstracts/Aalborg/TD(14)10053.pdf.

[11] Jonas Hansryd, Jonas Edstam, Bengt-Erik Olsson and Christina Larsson. Non-line-of-sight microwave backhaul for small cells. 2014.

[12] Hao Xu, V. Kukshya, and T.S. Rappaport. Spatial and temporal characteristics of 60-ghz indoor channels. *Selected Areas in Communications, IEEE Journal on*, 20(3):620–630, Apr 2002.

[13] T. Zwick, T.J. Beukema, and Haewoon Nam. Wideband channel sounder with measurements and model for the 60 ghz indoor radio channel. *Vehicular Technology, IEEE Transactions on*, 54(4):1266–1277, July 2005.

[14] AJ Motley and JMP Keenan. Personal communication radio coverage in buildings at 900 mhz and 1700 mhz. *Electronics Letters*, 24(12):763–764, 1988.

[15] COST 231. Digital mobile radio. towards future generation systems: Final report (chapter 4). Technical report, COST, 1999.